macQsimal	Title	Deliverable Number
	Tests of sensitivity of imager for THz sources	**D7.6**
Project Number **820393**		Version **1**

H2020-FETFLAG-2018-2021

macQsimal

Miniature Atomic vapor-Cell Quantum devices for SensIng and Metrology AppLications

Deliverable 7.6

Tests of sensitivity of imager for THz sources

WP7 – Atomic GHz & THz sensors and vector imagers

Authors: Shuying Chen (UDUR), Kevin Weatherill (UDUR)

Lead participant: UDUR

Delivery date: 10 August 2021

Dissemination level: Public

Type: R (Document, Report)

macQsimal	Title	Deliverable Number
	Tests of sensitivity of imager for THz sources	**D7.6**
Project Number **820393**		Version **1**

Revision History

Author Name (Partner short name)	Description	Date
Shuying Chen (UDUR) Kevin Weatherill (UDUR)	Draft deliverable	16.07.2021
Shuying Chen (UDUR) Lucy Downes (UDUR) Kevin Weatherill (UDUR)	Revisions and UDUR-internal review	28.07.2021
Philipp Treutlein (UNIBAS)	Review	29.07.2021
Shuying Chen (UDUR)	Final version	29.07.2021
Johannes Ripperger (accelCH)	Formal and layout checks	06.08.2021

Abbreviations

AMC   Amplifier multiplier chain

Cs   Caesium

FET   Field-effect transistors

FPA   Focal plane array

fW   Femto Watt

Hz   Hertz

IR   Infrared

K   Potassium

kHz   Kilo Hertz

Li   Lithium

µW   Micro-watt

MDP   Minimum detectable power

Na   Sodium

PDH   Pound-Drever-Hall

PSF   Point spread function

PTFE   Polytetrafluoroethylene

QCL   Quantum cascade laser

Rb   Rubidium

S&K   SCHÄFTER + KIRCHHOFF GmbH

THz   Terahertz

ULE   Ultra-low expansion

VCA   Voltage-controlled attenuator

WP   Work Package

Partner short names

accelCH   accelopment Schweiz AG, CH

CSEM   CSEM SA – Centre Suisse d'Électronique et de Microtechnique, CH

UDUR   University of Durham, UK

UNIBAS   Universität Basel, CH

macQsimal	Title	Deliverable Number
	Tests of sensitivity of imager for THz sources	**D7.6**
Project Number **820393**		Version **1**

Contents

Executive Summary

This deliverable is a report demonstrating our work towards the study of the sensitivity of our THz imaging system and make use of it for THz source testing. In the report, we introduce the field of THz imaging, noting key existing technologies and how these compare to our proposed Rydberg-based imaging system. We then show our achievement towards the goal of studying the sensitivity of the system, and then making use of this system to do the beam profiling test for the THz source.

Objectives of the Deliverable

The deliverable intends to introduce the test of the sensitivity and spatial resolution of our Rydberg atomic vapor cell based THz imaging setup we have built for THz source beam profiling.

Outcomes

Using thermal Rydberg atoms, we have successfully built a prototype THz imaging device with the spatial resolution of less than 1 mm, corresponding to the diffraction limit and the minimum detectable intensity is measured to be around $0.1 \, mW/m^2$ at 550 GHz. We were able to make use of this system for THz source beam profiling. We can clearly see the shape of the beam. And we were also able to get the Gaussian shape beam and did Gaussian fitting. It shows this imaging system can work as a real time, one-shot THz beam profiler.

Next steps

The next steps include:

1) Increasing the imaging area by increasing the light sheet size in the cell or the cell sizes.
2) Expand the technology to use multiple alkali elements in vapour cell as sensing medium in the imaging system. This will allow dual frequency imaging.
3) Develop more applications using this system, such as material characterisation, refractive index measurement and coating thickness measurement.
4) Incorporate the micro vapour cells fabricated by CESM, which will potentially make the system more compact and portable and reduce the effects of fringes in this coherent imaging scheme.

1 Introduction

Terahertz waves form a part of the electromagnetic spectrum in the frequency range from 100 GHz to 10 THz. It falls between microwave and infrared, the so-called 'THz gap' as shown in Figure 1. This frequency range is remarkable as it can penetrate various materials often associated with wrapping, such as plastic, fabric, paper, and card, but without damaging organic tissues as an x-ray would. This quality means that THz fields could prove useful for security tests, for example in airports or train stations [1], as well as in quality checking and defect detection [2, 3]. There is also interest in THz technology from the fields of biological and medical research for blood disease [4, 5] and oral cancer detection [6, 7]. So, THz imaging has wide potential applications in various fields [8].
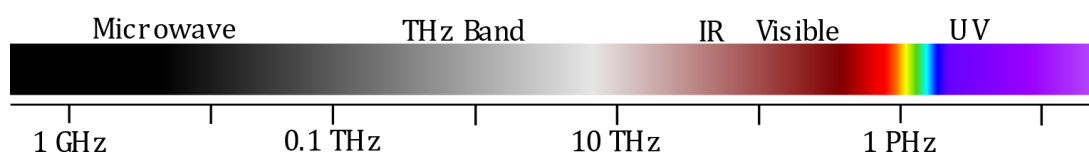
Figure 1: THz band gap.

However, THz imaging methods are in relative infancy as compared to microwave detection, with well-developed semiconductor technologies, or IR light detection with modern optical techniques. Currently, the principle methods of THz imaging include frequency up-conversion with nonlinear optical material such as diamond [9] or DAST crystal [10], transferring the THz field into optical photons; or single pixel capture method with Golay cells and bolometers or self-mixing in quantum cascade lasers (QCLs) [11]; or Focal Plane Arrays (FPAs), typically consisting of arrays of small point detectors such as micro bolometers [12,13], field-effect transistors (FETs) [14] or carbon nanotubes [15], or even superconductors [16]. These methods have different advantages, but the common drawback though, is that their THz imaging frame rate is severely limited, which restrains the practical applications of THz imaging.

At UDUR we have realised an ultra-fast THz imaging system with demonstrated frame rates over 3 kHz [17]. These frame rates are much faster than the traditional methods, e.g., thermodynamic THz detectors [12, 13] and may pave the way to the wider practical applications of THz imaging. The system uses a thermal alkali atomic vapour as an efficient THz to optical transducer. In our detection system, the difficult to detect THz frequency is transferred into easy to detect visible fluorescence. The fluorescence can be detected easily with normal cheap optical cameras. The benefit of using highly excited "Rydberg" atoms is that they have larger dipole moments to respond to the THz field and thus have higher sensitivity. In addition, the alkali atoms, including K, Rb, Cs, have hundreds of Rydberg levels which can be coupled to different THz frequencies, as shown in Figure 2. The vapour alkali cell is also easy to fabricate with low cost for K, Rb and Cs atoms. Thus, our system provides a novel easy and cheap THz imaging method with ultrafast speed.
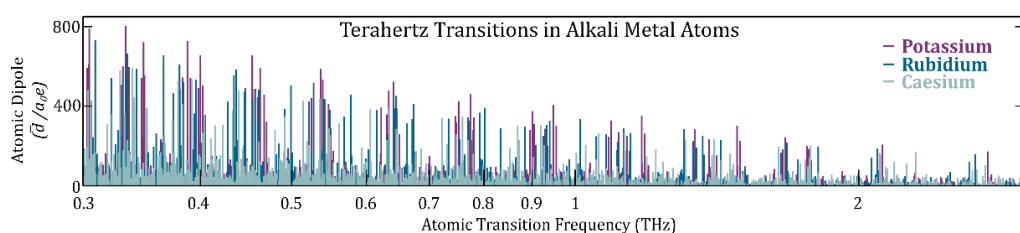
Figure 2: Useful transitions in K, Rb, Cs atoms for the different THz frequency couplings [18, 19]. The y-axis is the calculated atomic dipole moment, and the x-axis is the THz frequency of the transition.

To extend the application of this THz imaging system, the sensitivity and spatial resolution needs to be studied. Here we report the sensitivity of 190 fW per pixel per second and spatial resolution of 1 mm. We also demonstrate beam profiling for THz source (VDI).

2 Rydberg imaging system outline

We make use of the thermal Cs Rydberg atomic ensemble to realise the THz field imaging. The principle is that we utilise a three-step IR laser excitation to prepare the Cs atoms to a Rydberg state. When the THz field is turned on, the Cs Rydberg atoms are coupled to another specific Rydberg state. The states' energy difference is just the THz field energy. The atoms in that THz Rydberg state then decay to lower energy levels and finally to the ground states. Without the THz coupling, the atoms in the original Rydberg states will decay via several paths to the ground states, thus radiate different wavelength photons, showing visible orange fluorescence from the mixture of wavelengths from the different decaying paths. However, when the THz is on, the atoms are in another Rydberg state, and a particular decay path is strongly enhanced. The atomic cell radiates bright green fluorescence. People can use normal optical cameras to capture the fluorescence from the cell to provide spatial information of the THz field.
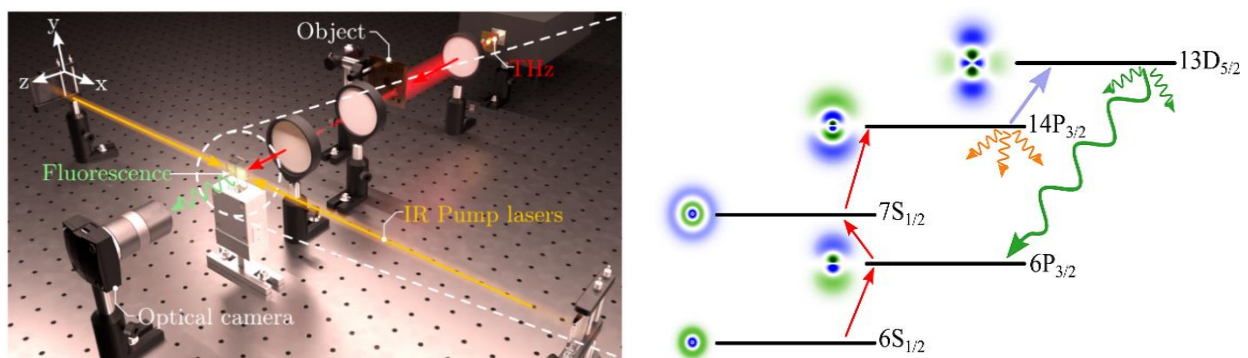
Figure 3: THz imaging experimental setup (left) and Cs atomic energy levels used (right) [17].

The energy levels of Cs atoms used are shown as the right figure in Figure 3 [17]. The three excitation steps are as below. The Cs atoms from ground state of $6S_{1/2}$ are excited to $6P_{3/2}$ with a first laser of wavelength 852 nm, and then from $6P_{3/2}$ excited to $7S_{1/2}$ with a second laser of wavelength 1470 nm, and finally $7S_{1/2}$ is excited to high excited Rydberg state $14P_{3/2}$ with the third laser 843 nm. After the atoms are prepared in the high Rydberg state, a THz field of frequency 0.55 THz is used to resonantly couple the levels $14P_{3/2}$ to another Rydberg level $13D_{5/2}$, resulting in the emission of strong green fluorescence from the decay path from $13D_{5/2}$ to $6P_{3/2}$. The centre wavelength of the fluorescence is 535 nm, which is captured by the optical camera.

The schematic of the imaging system experimental setup is shown in the left panel of Figure 3 [17]. The Cs vapour is contained within a cuboid quartz cell and heated to 50 Celsius degrees with a resistive metal-ceramic heater. The outer size of the cell is 10 mm × 10 mm × 50 mm. The atoms are prepared using co-axial IR laser beams shaped such that a 100 μm thick sheet of excited atoms is formed in the xy plane. The third laser 843 nm counter-propagates with the first and second lasers to reduce the Doppler Effect. The three lasers run continuously, and the first two lasers are frequency-stabilised with the sub-Doppler polarisation spectroscopy [20], while the third laser is now stabilised to a ULE cavity using PDH locking. The continuous-wave THz field (up to 19 μW at 0.55 THz) is emitted from a microwave-seeded amplifier multiplier chain (AMC) and propagates in the z direction, perpendicular to the plane of the vapour. And then the THz field is imaged on that atomic area after going through the object and a PTFE aspherical lenses imaging system (as in Figure 3). The fluorescence emitted by atoms when the THz is on is re-imaged onto an optical camera, providing an image of the incident THz field with the information of the object shape. Narrow band optical filters are used to increase the signal to noise ratio.
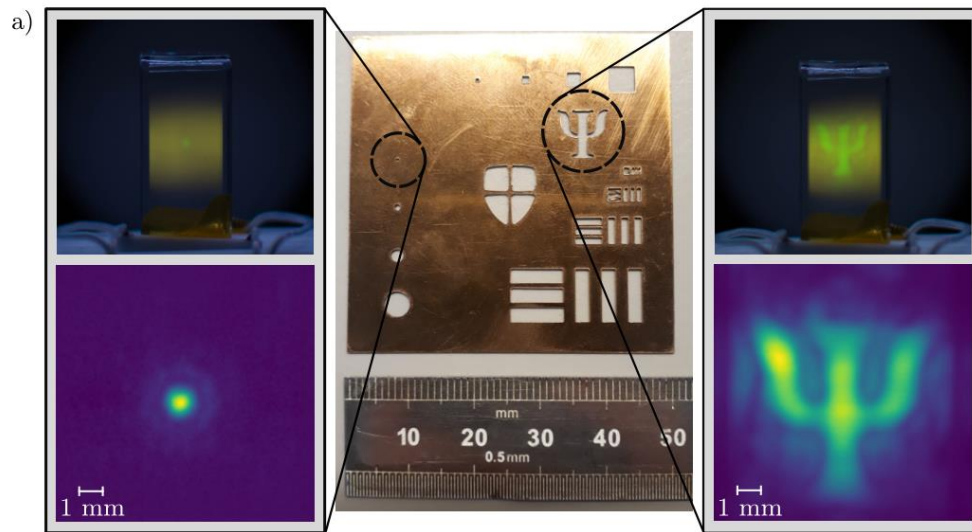
Figure 4: THz images taken using a metallic transmission test card [17]. A metal mask (centre) placed in the object plane of the system. Top left and right are true-colour images taken for a 0.50-mm-diameter pinhole (left) and a "Ψ"-shaped aperture (right). Down left and right are the images with narrow band filters in the system for 535 nm wavelength to increase the signal to noise ratio.

This real-time high resolution THz imaging system are useful for multiple applications, for example for the THz source beam profiling. In the next section, we introduce the sensitivity and spatial resolution of this THz imaging system, and then the results for the beam profiling for the test of THz source.

3 Sensitivity and spatial resolution of the THz imager

We studied the sensitivity and spatial resolution of the imaging system first in Sec. 3.1, then made use of the imaging system for one-go beam profiling for the THz source (VDI) in Sec. 3.2.

3.1 Sensitivity and spatial resolution

The imaging sensitivity is characterised with the minimum detectable power (MDP), which is the minimum THz power at which the resulting optical signal is reliably detectable above the noise floor of the instrument. The signal in the imaging is defined as the pixel value resulting from fluorescence in the presence of the THz field minus that from background fluorescence in the absence of the THz field, THz_{on} – THz_{off}. The signal from the $40 \times 40 \ \mu m^2$ pixel close to the centre of the image and its uncertainty are plotted against the incident THz power in Figure 5 [22]. From Figure 5, we see the system responds linearly for THz powers up to around 20 pW per $40 \times 40 \ \mu m^2$ pixel, as indicated by the green line. Above this value, the system experiences saturation, and we observe a smaller increase in signal for a given increase in THz power, which is seen as the deviation from the linear trend at high THz powers in Figure 5(a). The MDP is defined by considering the signal in the region of lowest incident THz power, shown in Figure 5(b). We average over 5 frames, each with an exposure of 200 ms. The MDP of our system is achieved as 190±30 fW*s^{-1}per $40 \times 40 \ \mu m^2$ pixel, or a minimum detectable intensity of 0.12 ±0.02 mW m^{-2}s^{-1}. This value shows an improvement of over 2 orders of magnitude on other room temperature imaging systems [23].
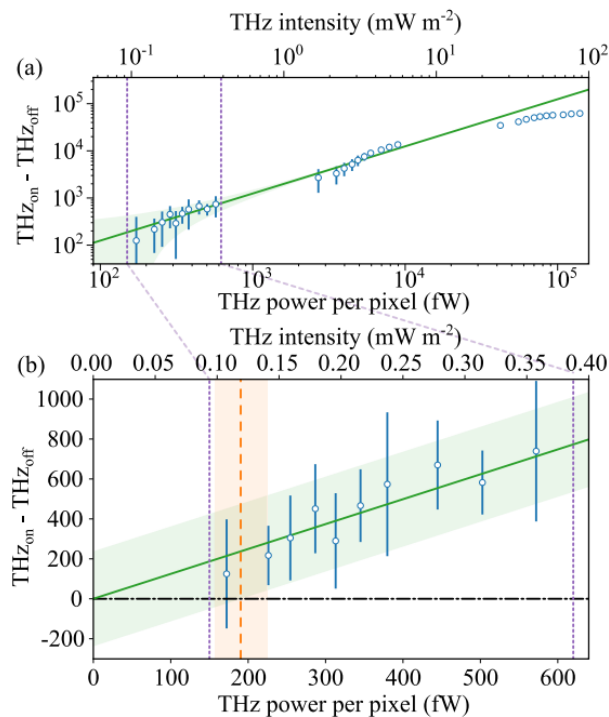
Figure 5: Minimum detectable power [17]. (a) The fluorescence signal $THz_{on} - THz_{off}$ (open blue circles) as a function of incident THz power for a total integration time of 1s. The linear trendline is extrapolated from that in panel (b) to highlight the saturation point at THz powers above 20 pW per $40 \times 40 \ \mu m^2$ pixel. The vertical dashed lines highlight the range of the data used in panel (b). (b) Plotting the measured fluorescence signal (open blue circles), we can map the linear response of the system (solid green line) plus its associated uncertainty (green shaded region) to the point at which the fluorescence signal is no longer reliably detectable (dashed orange line), at 190±30 fW per $40 \times 40 \ \mu m^2$ pixel for a 1s integration time.

To study the spatial resolution, we consider imaging a 0.50-mm diameter pinhole to be the point spread function (PSF) of the system, then compare the performance to that of an ideal imaging system. Because the diameter of the pinhole is smaller than the THz wavelength, the pinhole can be treated as a point source and hence the ideal intensity distribution can be given by an Airy pattern [24]. Based on the characteristics of the THz lenses, the f-number is calculated to be 1.5. The real and ideal unaberrated PSF are normalised to make the total power in each image equal. A radial average about the point of peak intensity is performed and the results are plotted in Figure 6. With the ratio of the maximum peak heights, a Strehl ratio for our system is achieved 0.57, indicating a moderate aberration of this imaging system, which arises from the simple design of the THz lenses used.

Two 0.50-mm-diameter pinholes separated by 1.00 mm are imaged for spatial resolution demonstration in Figure 6(b). In Figure 6(b), the two distinct apertures are clearly resolved in the images, which provides an upper bound of 1.00 mm on the system's spatial resolution, as near-diffraction-limited resolution. The experimental image matches the simulated image.
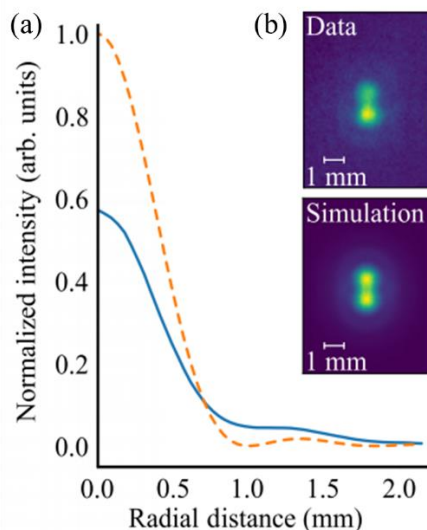
Figure 6: Demonstration of spatial resolution [17]. (a) Radially averaged intensity profiles of the measured PSF (solid blue line) and the simulated ideal PSF (dashed orange line). Both PSFs were scaled such that the total power in each image was equal. The ratio of peak heights gives a Strehl ratio of 0.57. (b) Experimental (top panel) and simulated (bottom panel) images of two 0.50-mm-diameter pinholes separated by 1.00 mm.

3.2   Beam profiling for THz source

Next, we test the imager used for THz source beam profiling. The THz source used here is VDI AMC seeded by an external microwave source. We use one Teflon lens placed at its focal length from the horn output to collimate the THz beam, then a second Teflon lens positioned at its focal length from the cell to focus the beam into the cell. Two 5 mm thick Nylon attenuators are used in the THz beam to reduce intensity and avoid saturation effects with the atomic vapour. We varied a voltage-controlled attenuator (VCA) to change the THz power as we record THz images in the cell. For every THz on image, a 'background' image was taken with the THz source turned off. These background images are subtracted from the THz on images to get rid of the background noise.
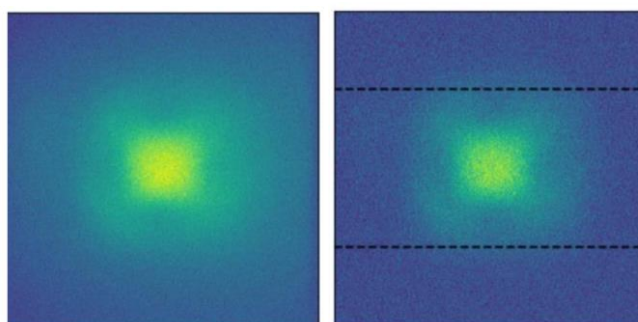
Figure 7: Images of THz source output. Raw image (left) and background subtracted image (right).

Figure 7 shows the images of the THz source output. On the left is a raw image of the beam from the THz source and the right figure is image subtracting the background, which shows clearer shape of the image. We can see the horn output profile is a square shape, not a perfect 2D Gaussian, while the shape of the horn aperture is rectangular [25].

In order to do the beam profiling, we select a region across the centre of the image in the right panel of Figure 7 and calculate an average pixel value across this region in the vertical direction. The horizontal dashed lines in the graph show the region we picked. Then we plot these average values as a function of

VCA voltage (inversely related to THz power) and we see the following Gaussian-like shapes in Figure 8 (a). In Figure 8(b) we fit a single 1D Gaussian to one average slice and from that the beam size can be extracted. Through the not perfect fitting, we can tell horn output is not perfectly Gaussian.
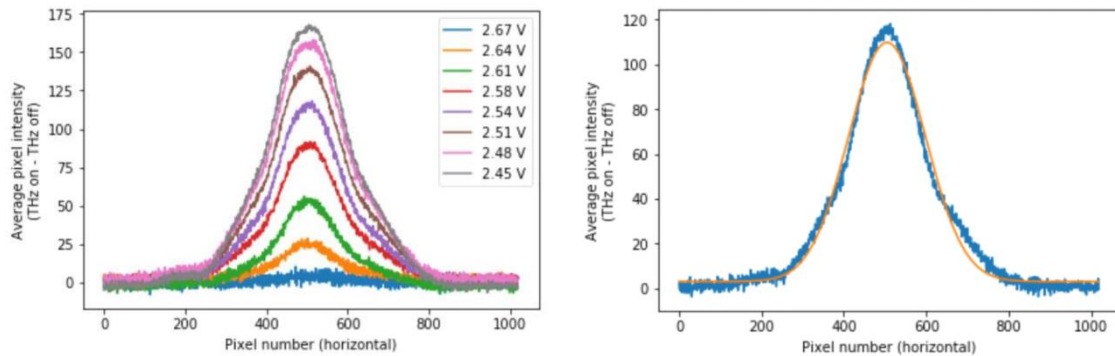
Figure 8: (a) Average pixel intensity versus UCA voltage (inversely related to THz power). (b) Gaussian fit to the beam profile.

In conclusion, we have successfully built a prototype device of THz imaging in the lab with the spatial resolution of 1mm, corresponding to the diffraction limit, while minimum detectable power is 190 fW per pixel. And we were able to make use of this THz imager to do beam profiling of the THz source. We can clearly see the shape of the horn and by adjusting the power and focal position, we are able to get the Gaussian-shape beam profile of the THz.

4 Future plan

After successfully realising the thermal Rydberg atomic THz imaging system, we made use of the imager to do the THz source beam profiling test. Thus, it is very interesting to develop more applications with following explorations as the future plan:

1) Develop multiple sizes of light sheet for larger image area for THz imaging.
2) Continue setting up a Rb system for THz imaging with the fibre-coupled line generators, which will be sensitive to more THz frequencies.
3) Test the micro vapour cells fabricated by CSEM. With the microcells, we can couple the lasers through the same window of the cell, and it is possible to make the system become more compact.
4) Develop the refractive index measurement for different materials with the THz imager.

References

[1] Kemp, Michael C., *et al.,* "Security applications of terahertz technology." *Terahertz for Military and Security Applications.* Vol. 5070. International Society for Optics and Photonics, 2003.

[2] Ellrich, Frank, *et al.,* "Terahertz quality inspection for automotive and aviation industries." *Journal of Infrared, Millimeter, and Terahertz Waves,* 41.4 (2020): 470-489.

[3] Ahi, Kiarash, and Mehdi Anwar. "Advanced terahertz techniques for quality control and counterfeit detection." *Terahertz Physics, Devices, and Systems X: Advanced Applications in Industry and Defense.* Vol. 9856. International Society for Optics and Photonics, 2016.

[4] Danciu, Mihai, *et al.,* "Terahertz spectroscopy and imaging: a cutting-edge method for diagnosing digestive cancers." *Materials*, 12.9 (2019): 1519.

[5] Wan, Min, John J. Healy, and John T. Sheridan. "Terahertz phase imaging and biomedical applications." *Optics & Laser Technology*, 122 (2020): 105859.

[6] Pawar, Ashish Y., *et al.,* "Terahertz technology and its applications." *Drug invention today,* 5.2 (2013): 157-163.

[7] Sim, Yookyeong Carolyn, *et al.,* "Terahertz imaging of excised oral cancer at frozen temperature." *Biomedical optics express*, 4.8 (2013): 1413-1421.

[8] Mittleman, Daniel M., "Perspective: Terahertz science and technology." *Journal of Applied Physics,* 122.23 (2017): 230901.

[9] Clerici, Matteo, *et al.,* "CCD-based imaging and 3D space–time mapping of terahertz fields via Kerr frequency conversion." *Optics letters,* 38.11 (2013): 1899-1901.

[10] Fan, Shuzhen, *et al.,* "Diffraction-limited real-time terahertz imaging by optical frequency up-conversion in a DAST crystal." *Optics Express*, 23.6 (2015): 7611-7618.

[11] Dean, Paul, *et al.,* "Absorption-sensitive diffuse reflection imaging of concealed powders using a terahertz quantum cascade laser." *Optics Express,* 16.9 (2008): 5997-6007.

[12] Lee, Alan WeiMin, and Qing Hu. "Real-time, continuous-wave terahertz imaging by use of a microbolometer focal-plane array." *Optics letters*, 30.19 (2005): 2563-2565.

[13] Lee, Alan WM, *et al.,* "Real-time imaging using a 4.3-THz quantum cascade laser and a 320/spl times/240 microbolometer focal-plane array." *IEEE Photonics Technology Letters*, 18.13 (2006): 1415-1417.

[14] Qin, Hua, *et al.,* "Room-temperature, low-impedance and high-sensitivity terahertz direct detector based on bilayer graphene field-effect transistor." *Carbon,* 116 (2017): 760-765.

[15] Suzuki, D., S. Oda, and Y. Kawano. "A flexible and wearable terahertz scanner." *Nature Photonics,* 10.12 (2016): 809-813.

[16] Ariyoshi, Seiichiro, *et al.,* "Superconducting detector array for terahertz imaging applications." *Japanese journal of applied physics,* 45.10L (2006): L1004.

[17] Downes, Lucy A., *et al.,* "Full-Field Terahertz Imaging at Kilohertz Frame Rates Using Atomic Vapor." *Physical Review X,* 10.1 (2020): 011027, and DOWNES, LUCY, ALEXANDRA (2020) A High-speed THz Imaging System based on THz-to-optical Conversion in Atomic Vapour, Durham theses, Durham University. Available at Durham E-Theses Online: http://etheses.dur.ac.uk/13797/.

[18] N. Šibalić, J. D. Pritchard, K. J. Weatherill, C. S. Adams, "ARC: An open-source library for calculating properties of alkali Rydberg atoms", *Computer Physics Communications*, 220, 319 (2017) https://doi.org/10.1016/j.cpc.2017.06.015

[19] C. Wade, N. Šibalić, N. de Melo, *et al.*, "Real-time near-field terahertz imaging with atomic optical fluorescence" *Nature Photon*, 11, 40–43 (2017).

[20] Khosrofian, John M., and Bruce A. Garetz. "Measurement of a Gaussian laser beam diameter through the direct inversion of knife-edge data." *Applied optics,* 22.21 (1983): 3406-3410.

[21] Carr, Christopher, Charles S. Adams, and Kevin J. Weatherill. "Polarization spectroscopy of an excited state transition." *Optics Letters*, 37.1 (2012): 118-120.

[22] I. G. Hughes and T. P. A. Hase, "Measurements and their Uncertainties" Oxford University, New York, 2010.

[23] F. Simoens and J. Meilhan, "Terahertz Real-Time Imaging Uncooled Array Based on Antenna- and Cavity-Coupled Bolometers" *Phil. Trans. R. Soc. A,* 372, 20130111 (2014).

[24] C. S. Adams and I. G. Hughes, "Optics f2f, from Fourier to Fresnel" Oxford University, New York, 2019.

[25] https://vadiodes.com/VDI/pdf/VDI%20Feedhorn%20Summary%202006_05.pdf.